1521-0103/379/2/191–202$35.00
THE JOURNAL OF PHARMACOLOGY AND EXPERIMENTAL THERAPEUTICS

https://doi.org/10.1124/jpet.121.000840
J Pharmacol Exp Ther 379:191–202, November 2021

Identification and Characterization of Two Structurally Related Dipeptides that Enhance Catalytic Efficiency of Neurolysin[S]

Srinidhi Jayaraman,[1] Joanna Kocot,[1] Shiva Hadi Esfahani,[1] Naomi J. Wangler, Arzu Uyar, Yehia Mechref, Paul C. Trippier, Thomas J. Abbruscato, Alex Dickson, Hideki Aihara, David A. Ostrov, and Vardan T. Karamyan

Department of Pharmaceutical Sciences (S.J., J.K., S.H.E., N.J.W., T.J.A., V.T.K.) and Center for Blood Brain Barrier Research (T.J.A., V.T.K.), School of Pharmacy, Texas Tech University Health Sciences Center, Amarillo, Texas; Department of Biochemistry and Molecular Biology, Michigan State University, East Lansing, Michigan (A.U., A.D.); Department of Chemistry and Biochemistry, Texas Tech University, Lubbock, Texas (Y.M.); Department of Pharmaceutical Sciences, College of Pharmacy and Center for Drug Discovery, University of Nebraska Medical Center, Omaha, Nebraska (P.C.T.); Department of Biochemistry, Molecular Biology and Biophysics, University of Minnesota, Minneapolis, Minnesota (H.A.); and Department of Pathology, Immunology and Laboratory Medicine, University of Florida, Gainesville, Florida (D.A.O.)

Received July 12, 2021; accepted August 10, 2021

ABSTRACT

Neurolysin (Nln) is a recently recognized endogenous mechanism functioning to preserve the brain from ischemic injury. To further understand the pathophysiological function of this peptidase in stroke and other neurologic disorders, the present study was designed to identify small molecule activators of Nln. Using a computational approach, the structure of Nln was explored, which was followed by docking and in silico screening of ~140,000 molecules from the National Cancer Institute Developmental Therapeutics Program database. Top ranking compounds were evaluated in an Nln enzymatic assay, and two hit histidine-dipeptides were further studied in detail. The identified dipeptides enhanced the rate of synthetic substrate hydrolysis by recombinant (human and rat) and mouse brain–purified Nln in a concentration-dependent manner (micromolar A_{50} and $A_{max} \geq 300\%$) but had negligible effect on activity of closely related peptidases. Both dipeptides also enhanced hydrolysis of Nln endogenous substrates neurotensin, angiotensin I, and bradykinin and increased efficiency of the synthetic substrate hydrolysis (V_{max}/K_m ratio) in a concentration-dependent manner. The dipeptides and competitive inhibitor dynorphin A (1-13) did not affect each other's affinity for Nln, suggesting differing nature of their respective binding sites. Lastly, drug affinity responsive target stability (DARTS) and differential scanning fluorimetry (DSF) assays confirmed concentration-dependent interaction of Nln with the activator molecule. This is the first study demonstrating that Nln activity can be enhanced by small molecules, although the peptidic nature and low potency of the activators limit their application. The identified dipeptides provide a chemical scaffold to develop high-potency, drug-like molecules as research tools and potential drug leads.

SIGNIFICANCE STATEMENT

This study describes discovery of two molecules that selectively enhance activity of peptidase Nln—a newly recognized cerebroprotective mechanism in the poststroke brain. The identified molecules will serve as a chemical scaffold for development of drug-like molecules to further study Nln and may become lead structures for a new class of drugs. In addition, our conceptual and methodological framework and research findings might be used for other peptidases and enzymes, the activation of which bears therapeutic potential.

Introduction

Several recent experimental studies have suggested that peptidase neurolysin (Nln) is a compensatory, cerebroprotective mechanism in the poststroke brain that functions to process a number of neuropeptides to reduce excitotoxicity, oxidative stress, edema formation, blood brain-barrier hyperpermeability, and neuroinflammation (Karamyan, 2019; Karamyan, 2021b). Nln (EC 3.4.24.16) is a zinc endopeptidase from M3 family of peptidases (Dauch et al., 1995) that is most studied for hydrolytic processing of bioactive peptides in the

This study was funded by National Institutes of Health National Institute of Neurological Disorders and Stroke [Grant R01NS106879] with additional support from TTUHSC School of Pharmacy. Discovery of small molecule activators of Nln described herein is the subject of a published patent application: PCT Int. Appl. (2020) WO2020047185.

No author has an actual or perceived conflict of interest with the contents of this article.

[1]S.J., J.K., and S.H.E. contributed equally to this work.

https://doi.org/10.1124/jpet.121.000840.

[S] This article has supplemental material available at jpet.aspetjournals.org.

ABBREVIATIONS: ACE, angiotensin converting enzyme; ACE2, angiotensin converting enzyme 2; aCSF, artificial cerebrospinal fluid; Ang I, angiotensin I; BK, bradykinin; BSA, bovine serum albumin; DARTS, drug affinity responsive target stability assay; DSF, differential scanning fluorimetry; NCI DTP, National Cancer Institute Developmental Therapeutics Program; NEP, neprilysin; Nln, neurolysin; NT, neurotensin; QFS, quenched fluorescence substrate; TOP, thimet oligopeptidase.

extracellular environment (Checler and Ferro, 2018; Shrimpton et al., 2002). The main neuropeptides inactivated by Nln (bradykinin, substance P, neurotensin, angiotensin II) are neurotoxic/cerebrotoxic in the acute postischemic brain, whereas the peptides generated by Nln [angiotensin-(1–7), Leu- and Met-enkephalins] are deemed to be neuroprotective/cerebroprotective. Notably, expression of Nln is upregulated in primary cortical neurons and mouse brain after ischemia, suggesting its compensatory function (Rashid et al., 2010; Rashid et al., 2014). Inhibition of Nln after stroke leads to aggravation of the disease outcomes in mice, whereas overexpression of Nln in the mouse brain prior to stroke affords profound cerebroprotection (Jayaraman et al., 2020). The ability of Nln to process a diverse group of neuropeptides suggests that it could potentially serve as a single therapeutic target to modulate the function of multiple targets that are critically involved in various mechanisms of brain injury or cerebroprotection and restoration. To be able to test this hypothesis and further understand the pathophysiological function of this peptidase in stroke and other neurologic disorders, the present study was designed with a purpose of identifying small molecule activators of Nln. Here, we describe discovery of two structurally related dipeptides that selectively enhance catalytic efficiency of Nln. We present results of detailed in vitro pharmacological studies used to document and confirm the phenomenon of Nln activation for the first time. The identified dipeptides will serve as a scaffold for development of high-potency Nln activators to study the activation mechanism of the peptidase and its functional significance in pathogenesis of stroke and other neurologic disorders. If the therapeutic potential of Nln activators is confirmed in future studies, these molecules might become a new class of drugs.

Materials and Methods

Molecular Docking. Candidate small-molecule modulators of Nln were selected based on a strategy used for discovery of allosteric enhancers of peptidase ACE2 (Hernandez Prada et al., 2008; Kulemina and Ostrov, 2011). ACE2 and Nln undergo conformational changes involving large hinge-bending motions when the apo form transitions to substrate-bound forms. A unique structural pocket in ACE2 located at the hinge region of the catalytic domain in the apo form was previously used as a target for molecular docking and selection of small molecules that enhance the catalytic activity of ACE2 (Hernandez Prada et al., 2008; Kulemina and Ostrov, 2011). In the current study, structural analysis of the hinge region of Nln in its open conformation was carried out using DSSP (Kabsch and Sander, 1983) and castP (Dundas et al., 2006) to identify structural pockets with adequate solvent accessible volumes and chemical characteristics for binding of drug-like small molecules [molecular weight <500; octanol/water partition coefficients <5; H-bond donors <5; H-bond acceptors <10 (Lipinski et al., 2001)]. One potentially druggable site was selected in the hinge region of Nln in its open conformation (formed by R164, K168, L306, R514, N519, E521, T522 residues of the full-length rat Nln), and programs implemented in the DOCK program package (UCSF) were used to generate files for molecular docking. SPHGEN was used to place spheres at sites that represent potential ligand atoms in the selected hinge site, and GRID was used to calculate scoring grids with a box size 5 Å from the selected spheres. DOCK 6.5 (UCSF) was used to dock and rank 139,725 compounds from the National Cancer Institute Developmental Therapeutics Program (NCI DTP) repository (http://zinc.docking.org/catalogs/ncip). The experiment was completed in the University of Florida High Performance Computing Facility by parallel processing. Compounds were selected to include protonation variants at medium pH 5.75–8.25. Each molecule was positioned into the selected surface pocket in 1000 different orientations and scored with rank based on the predicted polar (H-bonding) and nonpolar (van der Waals) interactions. Top-scoring 40 compounds were obtained from NCI DTP and used for primary screening (see below).

Recombinant Rat Nln. N-terminal polyhistidine-tagged recombinant rat Nln was produced in *Escherichia coli* using a plasmid construct in pBAD/His vector system (Invitrogen) kindly provided by Dr. David W. Rodgers (University of Kentucky) (Lian et al., 2000; Brown et al., 2001). Production and purification of the recombinant peptidase was carried out essentially as described in our previous publication (Wangler et al., 2016). Purity of recombinant Nln (≥95%) was verified by SDS-PAGE and size exclusion chromatography, whereas identity was confirmed by Western blotting using a specific anti-Nln antibody (product RP3-Neurolysin, TriplePointBiologics) (Wangler et al., 2012; Rashid et al., 2014). Specific activity of recombinant Nln was determined by an enzymatic assay described below.

Recombinant Human Peptidases. Recombinant human Nln and thimet oligopeptidase were produced in-house following the same procedure described for rat Nln. Human neprilysin (NEP; product 1182-ZNC), ACE (product 929-ZN), and ACE2 (product 933-ZN) were purchased from R&D systems. For drug affinity responsive target stability (DARTS) and differential scanning fluorimetry (DSF), which required much higher quantities of recombinant protein, NEP was obtained from Sino Biologic (product 10805-H07H).

Mouse Brain Nln. P10 mouse forebrains were used for purification of native Nln because expression of the peptidase is about five times higher at this age compared with adult mouse forebrain (Rashid et al., 2010; Wangler et al., 2012). In brief, forebrains were homogenized in hypotonic buffer (20 mM $NaPO_4$, pH 7.2) followed by gentle sonication and centrifugation (30 minutes at 48,000 × g at 4°C). The resulting supernatant was filtered through a 100-kDa cutoff centrifugal filtering unit and concentrated in a 30-kDa cutoff centrifugal filtering unit (Amicon Ultra; Millipore). Nln was semipurified from the concentrate by size exclusion chromatography using a Superdex 200 Increase 10/300 GL column (GE Healthcare) in AKTA Purifier FPLC system (GE Healthcare). Elution of Nln was tracked by the enzymatic assay described below, and the fraction with the highest Nln activity was directly used for the experiments.

Enzymatic Assays. Activity of Nln was measured in a continuous assay by documenting the increase in fluorescence occurring upon cleavage of a quenched fluorescence substrate (QFS) Mca-Pro-Leu-Gly-Pro-D-Lys(DNP)-OH (product M-2270, Bachem Peptides) (Dauch et al., 1991a; Rashid et al., 2014). In brief, a fixed concentration of recombinant or mouse brain–purified Nln was incubated with 15 μM (for primary screening and determination of A_{50} values) or 2.5–75 μM (for determination of K_m and V_{max} values) QFS in artificial cerebrospinal fluid (aCSF; NaCl 126 mM, $NaHCO_3$ 26 mM, KCl 3 mM, KH_2PO_4 1.4 mM, HEPES 25 mM, glucose 4 mM, $MgCl_2$ 1.3 mM, $CaCl_2$ 1.4mM, $ZnSO_4$ 0.2 μM, pH 7.2) containing 0.01% final assay concentration of Triton X-100 at 37°C. In experiments involving dynorphin A (1-13), a fixed concentration of rat recombinant Nln was incubated with 15 μM QFS and varying concentrations of dynorphin A (1-13) in the absence or presence of one of the activators at 100 μM. In the reverse experiment, a fixed concentration of rat recombinant Nln was incubated with 15 μM QFS and varying concentrations of one of the activators in the absence or presence of dynorphin A (1-13) at 1 μM. All assays were initiated by addition of QFS (100 μl assay volume in 96-well plates), and each experimental sample was present in duplicate. Generation of the fluorescent product (Mca-Pro-Leu-OH; λ_{ex} = 320, λ_{em} = 405) was documented every 1 minute in a plate reader (SynergyMX; Biotek) at initial velocity conditions wherein ~10% of the substrate was metabolized. For mouse brain–purified Nln, Pro-Ile–inhibited (10 mM final assay concentration) fraction of substrate hydrolysis was considered Nln-specific (Dauch et al., 1991b).

Activity of recombinant human TOP was assessed in the same way as for Nln except that the assay was carried out in the presence of

0.1 mM dithiothreitol (Shrimpton et al., 1997). Likewise, activities of recombinant human ACE, NEP, and ACE2 were measured similar to Nln except that quenched fluorescence substrate Mca-Arg-Pro-Pro-Gly-Phe-Ser-Ala-Phe-Lys(Dnp)-OH was used for ACE and NEP (Miners et al., 2008; Joyner et al., 2012), and Mca-Ala-Pro-Lys-(Dnp)-OH was used for ACE2 (Vickers et al., 2002) (both substrates at 10 μM final assay concentration; product BML-P227 and BML-P163, Enzo Life Sciences).

Primary Screening. The effect of top-ranked 40 compounds (obtained from NCI DTP) on activity of recombinant rat Nln was carried out at 10 and 100 μM final assay concentrations. All test compounds were dissolved in DMSO to make 10 to 50 mM stocks, which was followed by dilution in aCSF for working stocks. Presence of up to 3% DMSO did not substantially affect activity of the enzyme in our assays. The test compounds were incubated with Nln for 10 minutes at 37°C before addition of the substrate to start the reaction.

The two molecules identified to activate Nln in primary screen were additionally purchased from a commercial vendor (product G-2355 and G-4595, Bachem Peptides) and retested for activation of Nln using a broader concentration range (0.1 μM to 1 mM final assay concentrations). All subsequent experiments were carried out using the purchased dipeptides.

Endogenous Substrates of Nln and Mass-Spectrometry Analysis. Hydrolysis of neurotensin, bradykinin, and angiotensin I (20 μM; obtained from Phoenix Peptides) by recombinant rat Nln (0.5 nM in aCSF containing 0.01% Triton X-100) was carried out in the absence and presence of the two identified activators (at 40 and 100 μM) in a total volume of 30 μl at 37°C for 10 minutes. The reaction was stopped with 1 μl of 1.0 N HCl, which was followed by freezing at –80°C. LC-MS/MS analysis was performed on a Shimadzu Nexera Ultra High-performance LC system and triple quadrupole Ion-Trap AB SCIEX QTRAP 5500 mass spectrometer equipped with Kinetex-EVO-C18 100Å column (1.7 μm, 50 × 2.1 mm, Phenomenex) (Jayaraman et al., 2020). Solvent A (0.1% formic acid in water) and solvent B (0.1% formic acid in acetonitrile) were run at the following elution gradient at 300 μl/min flow rate: 5% solvent B over 0.1 minutes, and then held at 5% for 0.9 minutes, and this was followed by a 1.5-minute linear gradient to 50% B, reaching 80% B over 2 minutes and 95% over 0.2 minutes. The eluted peptides were ionized by electrospray ionization and analyzed in line using the mass spectrometer. For each peptide, the precursor ion of charged state calculated by m/z ratio, as M + 1, (M + 2)/2, or (M + 3)/3 were identified and fragmented by a collision-induced dissociation gas. Detection of bradykinin (BK) and its hydrolysis product BK-(1-5), neurotensin (NT) and its product NT-(1-10), and angiotensin I (Ang I) and its product Ang-(1-7), were performed in the positive polarity and multiple-reaction monitoring mode (50-millisecond dwell times and 5500 V). The collision energies used for NT, BK, Ang I, NT-(1-10), BK-(1-5), and Ang-(1-7), were 34, 40, 27, 50, 45, and 30 V, respectively. Synthetic peptide DAMGO (product 1171, Tocris Bioscience) was used as internal standard and spiked into each sample. For each peptide and the internal standard, two different mass transitions were measured. The Q_1 to Q_3 transitions were m/z 531.1 precursor ion to m/z 120.1 for BK and m/z 573.3 precursor ion to m/z 237.1 for BK-(1-5), m/z 558.4 precursor ion to m/z 136.3 for NT and m/z 642.3 precursor ion to m/z 136.3 for NT-(1-10), m/z 433.3 precursor ion to m/z 110.1 for Ang I and m/z 450.4 precursor ion to m/z 110.1 for Ang-(1-7), and m/z 514 precursor ion to m/z 134.1 for DAMGO. The peak areas for all peptides and the internal standard were obtained through Analyst software (version 1.7.2) and expressed as peak area ratio (peptide peak area/internal standard peak area). In each LCMS experiment, samples from all experimental groups were analyzed for each dipeptide separately (at two concentrations). The recorded peak area ratio of peptide/internal standard for "Nln alone" condition was arbitrarily set to 100%, and the peak area ratios of other experimental groups were compared with "Nln alone" values.

DARTS. DARTS assays were performed according to a previously described protocol (Lomenick et al., 2009) with some modifications. Briefly, 2.6 μM recombinant Nln or NEP was incubated with vehicle (aCSF), His-Tyr, or dynorphin A (1-13) (both at final concentrations of 30, 100, or 300 μM) in aCSF containing 0.01% Triton X-100 for 30 minutes at 37°C, and this was followed by addition of subtilisin A (Sigma-Aldrich product P4860) at 1:130 (subtilisin: protein; w/w) ratio. The digestion lasted 20 minutes at 37°C, and this was followed by immediate addition of protease inhibitor cocktail (HALT Protease Inhibitor Cocktail, product 78430, Thermo Scientific) to inhibit subtilisin A. As an additional control, an undigested sample of each peptidase, which received aCSF with 0.01% Triton X-100 instead of subtilisin A, was also used. After inhibition of digestion, all samples were treated with 4× Laemmli sample buffer, which was followed by immediate heating (90°C for 10 minutes), SDS PAGE gel electrophoresis, and conventional Western blotting as essentially described in our previous publications (Wangler et al., 2012, 2016). Primary antibodies used in these experiments were polyclonal anti-Nln or anti-NEP antibodies obtained from TriplePointBiologics (product RP1-Neurolysin and RP4-Neprilysin-1, used at 1:20,000 dilution). Visualization of immunoreactive bands was carried out using Pierce ECL 2 Western Blotting Substrate (Thermo Scientific), whereas densitometric analysis was carried out using Quantity One software (Bio-Rad Laboratories). Samples from all experimental groups for each peptidase/ligand were included in each SDS PAGE gel run; each gel included duplicates for "undigested control" (Nln incubated with vehicle but not subtilisin) and peptidase + subtilisin groups and a single sample for all other experimental groups. For each gel, the recorded density of bands representing the "undigested control" group was arbitrarily set to 100%, and the density values of other experimental groups were compared with "undigested control" values.

DSF. DSF was conducted using GloMelt Thermal Shift Protein Stability Kit (product 33021-T, Biotium) according to manufacturer's protocol. Briefly, total 20 μl of assay mixture containing 3 μM recombinant Nln or NEP in aCSF with 0.01% Triton X-100, His-Tyr, or dynorphin A (1-13) (both at final concentrations of 30, 100, or 300 μM), and 1X GloMelt dye were mixed in a 96-well PCR plate and read in CFX96 Touch Real-Time PCR Detection System (Bio-Rad). The reaction mixtures without an enzyme or ligand served as controls. The samples (each present in duplicate) were thermally denatured by heating from 25°C to 99°C at a ramp rate of 0.5°C/min, and SYBR/FAM filter setting (470 ± 20 nm excitation, 520 ± 10 nm emission) was used for readings at each heating step. Note that in experiments involving NEP, the manufacturer's buffer (20 mM MES, 100 mM NaCl, 1 mM $ZnCl_2$, 10% glycerol, pH 6.5) was replaced with aCSF containing 0.01% Triton X-100 to reduce fluorescence intensity fluctuations at the beginning of the melting curve (<35°C).

Statistical Analyses. Statistical analyses and curve fitting were conducted with GraphPad Prism 7.05 software. For each enzymatic reaction, slope of the line that represents the initial velocity (V_0) for the reaction progress curve was calculated using the liner regression model of the software (V_0 = slope = Δ fluorescent intensity of the reaction product/Δ time). For calculation of A_{50} and A_{max} values, V_0 values for QFS hydrolysis by Nln in the presence of varying concentrations of an activator were expressed as percentage within each experiment, with 100% being V_0 of enzymatic reaction in the absence of an activator (i.e., basal activity with vehicle control). A_{50} and A_{max} values were calculated by fitting $\%V_0$ values into a nonlinear regression model for the three-parameter log(stimulator) versus response equation [Y = bottom + (top − bottom)/(1 + 10^((LogEC$_{50}$ − X)))]. IC_{50} values for dynorphin A (1-13) were calculated by fitting initial velocity values for hydrolysis of QFS by Nln in the presence of varying concentrations of dynorphin A (1-13) into a nonlinear regression model for the three-parameter log(inhibitor) versus response equation [Y = bottom + (top − bottom)/(1 + 10^((X − LogIC$_{50}$)))]. K_i values were determined using the Cheng-Prusoff equation: $K_i = IC_{50}/(1 + S/K_m)$ in which S is the substrate concentration (15 μM QFS in our experiments) and K_m is the K_m value for the substrate (15 μM for QFS, see Table 3). K_m and V_{max} values were calculated by fitting initial velocity values for hydrolysis of varying concentrations of QFS by Nln in the absence or presence of 40 or 100 μM of each modulator into Michaelis-Menten

equation [$Y = V_{max}*X/(K_m + X)$]. Comparison of data from experiments with several groups (Figs. 5, 8, and 9) was done by one-way ANOVA followed by Dunnett's multiple comparison test. A P value <0.05 was considered statistically significant. Data are presented as mean, mean with 95% confidence intervals, or mean ± S.D.

Results

Molecular Docking. In this study, a structural analysis of the hinge region of Nln in its open conformation was carried out to identify a surface pocket that could be further explored as a modulatory binding site. A methodology originally developed for peptidase ACE2 (Hernandez Prada et al., 2008; Kulemina and Ostrov, 2011) was used here because Nln and ACE2 are structurally related and are classified as members of the neurolysin-like protein family, in which the N-terminal half of the structure is multihelical, and the C-terminal half contains the thermolysin-like catalytic domain. The search for a modulatory site was carried out in the hinge region because crystal structures of both Nln and ACE2 demonstrate that catalysis is accompanied by large hinge-bending motions (Brown et al., 2001; Towler et al., 2004). The hinge region in both peptidases can affect the distance between the two structural domains and by that modulate substrate binding and catalysis (Ray et al., 2004; Towler et al., 2004; Uyar et al., 2018). Several surface pockets with adequate solvent accessible volumes [DSSP (Kabsch and Sander, 1983) and castP (Dundas et al., 2006)] were identified in the hinge region of Nln. One of these pockets was selected as a potential site for molecular docking (Fig. 1) because it is located at a position analogous to the ACE2 site used for identification of small-molecule catalytic enhancers (Hernandez Prada et al., 2008; Kulemina and Ostrov, 2011). The selected surface pocket was used for molecular docking and virtual, high-throughput screening of drug-like compounds from NCI DTP, and this was followed by ranking of compounds based on their combined energy scores for hydrogen bonding and van der Waals contact interactions with the selected surface pocket (Table 1).

Primary and Secondary Screens. Top-ranking 40 compounds identified in the virtual screen were obtained from NCI DTP and used at 10 and 100 μM assay concentrations to evaluate their effects on hydrolysis of QFS by recombinant rat Nln (Table 2). Among tested compounds, there were more than a handful that showed inhibition of the peptidase at both concentrations, whereas two compounds (NSC 374121 and NSC 523374) showed a clear, concentration-dependent activation of Nln.

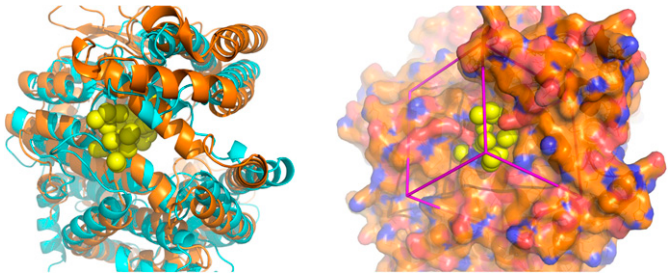

Fig. 1. Surface pocket in the hinge region selected for molecular docking. Left panel: superposition of ribbon diagrams of ACE2 (cyan) and Nln (orange) and their hinge regions. Crystal structures of the open conformations of both peptidases are shown (Brown et al., 2001; Towler et al., 2004). The yellow spheres represent the site in the hinge region of Nln selected for molecular docking. Right panel: the crystal structure of Nln shown in the same orientation as in the left panel. The molecular surface is colored gold for carbon, red for oxygen, and blue for nitrogen. Yellow spheres depict sites for potential ligand atoms used in molecular docking. The box in magenta represents the boundaries of the scoring grid used to generate scores that consider electrostatic (polar) and van der Waals (nonpolar) interactions.

Based on the results of the primary screen, compounds NSC 374121 and NSC 523374 (dipeptides *L*-histidyl-*L*-tyrosine and *L*-histidyl-*L*-histidine—referred to as His-Tyr and His-His throughout the text; Fig. 2) were purchased from a commercial vendor and retested for activation of Nln using a broad range of concentrations. Concentration-dependent effect of both compounds on initial velocity of QFS hydrolysis by Nln is presented in Fig. 2. For His-Tyr the calculated A_{50} was 89.7 μM (95% CI, 74.2–108.6 μM) and A_{max} was 449% (95% CI, 432%–468%). For His-His, the calculated average A_{50} was 136 μM (95% CI, 104–179 μM), and A_{max} was 463% (95% CI, 436%–492%).

Notably, these experiments were carried out in an assay buffer containing 0.01% Triton X-100, as recommended by Feng and colleagues (2005, 2007), to avoid identification of promiscuous modulators of enzymes. In addition, to further verify our observations and avoid identification of nonspecific modulators, the concentration-response experiments were also reproduced in the presence of 0.1% CHAPS or 0.01 mg/ml bovine serum albumin (BSA), instead of Triton X-100, as suggested by other investigators (Goode et al., 2008). In these experiments, the concentration-dependent effect of both dipeptides on activity of Nln was similar to the assay condition wherein Triton X-100 was present in aCSF (Supplemental Fig. 1, A and B).

The inherent fluorescence-enhancing or -quenching properties of His-Tyr and His-His were also verified to avoid false conclusions. In this set of experiments, it was determined that the dipeptides had negligible effect on the fluorescence signal recorded from the hydrolysis product of QFS [Mca-Pro-Leu-OH; (Dauch et al., 1991a)] under the same experimental conditions (Supplemental Fig. 1, C and D).

Additionally, we reproduced the observed effects of His-Tyr and His-His in several independently purified batches of recombinant rat Nln (unpublished data). Lastly, we purchased a structural analog of His-Tyr with reverse C- and N-terminal amino-acid sequence (i.e., Tyr-His; *L*-tyrosyl-*L*-histidine, product G-3415, Bachem Peptides) and tested for its effect on activity of Nln. In these experiments, the effect of Tyr-His was negligible compared with that of His-Tyr and His-His (Fig. 2).

Based on these collective observations, we determined that the effect of His-Tyr and His-His on activity of Nln was likely not an artifact and continued with more detailed pharmacological studies.

Species Selectivity of His-Tyr and His-His. To determine whether the observed effects of His-Tyr and His-His are only limited to the rat Nln, concentration-response studies were also carried out with human recombinant and mouse brain–purified Nln. Concentration-dependent effects of both compounds on initial velocity of QFS hydrolysis by human and mouse Nln were similar to that of the rat peptidase and are presented in Fig. 3. With human recombinant Nln, the calculated A_{50} for His-Tyr was 15.9 μM (95% CI, 13.0–19.3 μM), and A_{max} was 321% (95% CI, 313–330). For His-His, the calculated A_{50} was 35.1 μM (95% CI, 30.1–39.9 μM), and A_{max} was 332% (95% CI, 326%–338%). With mouse brain Nln, the calculated A_{50} for His-Tyr was 12.7 μM (95% CI, 8.9–17.9 μM), and A_{max} was 271% (95% CI, 258%–285%). For His-His, the calculated A_{50} was 0.22 μM (95% CI, 0.16–0.29 μM), and A_{max} was 276% (95% CI, 269%–283%).

TABLE 1
Top 10 scoring compounds for the selected surface pocket in the hinge region of Nln

Rank #	ID[a]	LogP	H-Donors	H-Acceptors	MW	VDW	ES	Score
1	NSC 42215[b]	2.41	0	3	184.234	19.338	−108.107	−88.767
2	NSC 353874	1.24	1	3	196.245	−9.700	−46.004	−55.705
3	NSC 128977	−0.03	2	6	272.174	8.901	−59.141	−50.239
5	NSC 359097	−1.65	2	3	169.178	3.290	−50.315	−47.025
6	NSC 14541	−0.52	2	4	228.38	−26.993	−19.369	−46.363
7	NSC 523374[c]	−1.71	5	8	292.296	−32.834	−11.721	−44.555
8	NSC 155877	−1.48	0	3	334.655	−23.804	−19.725	−43.529
10	NSC 302851	−5.51	4	6	240.291	−26.927	−15.557	−42.484
11	NSC 600947	1.72	1	3	239.403	−30.350	−12.113	−42.463
12	NSC 163084	−0.59	4	6	352.404	−34.094	−8.321	−42.416

ES, electrostatic interactions; MW, molecular weight; VDW, van der Waals interactions.
[a]NSC numbers are unique identifiers for compounds deposited in NCI DTP database which can be accessed at https://dtp.cancer.gov/dtpstandard/dwindex/index.jsp.
[b]NSC 42215 was also ranked #4 with combined score of −48.091 (was not screened in enzymatic assays because it was not available from NCI DTP or from a commercial vendor).
[c]NSC 523374 was also ranked #9 with combined score of −43.371. Note that ranking of a compound more than once indicates its predicted binding to Nln in more than one orientation.

Peptidase Selectivity of His-Tyr and His-His. In this set of experiments, concentration-dependent effects of His-Tyr and His-His on activity of peptidases related to Nln were studied (Fig. 4). Overall, both dipeptides demonstrated negligible to small effect on activity of TOP, ACE, ACE2, and NEP across a broad range of concentrations. Only at 300 μM concentration, His-Tyr statistically significantly inhibited activity of ACE by 15.5% (95% CI, 9.8%–21.3%). Similarly, in the presence of His-His, statistically significant inhibition was only observed for ACE (by 14.4%; 95% CI, 13.5%–15.4%) at 300 μM concentration of the dipeptide.

The Effect of His-Tyr and His-His on Hydrolysis of Endogenous Substrates. The use of synthetic substrates with fluorescence properties in enzymatic assays is very convenient because they allow easy tracking of the reaction progress (Novinec et al., 2014). However, observations made with synthetic substrates cannot be translated a priori to endogenous substrates because there are examples in scientific literature describing compounds that showed effects on enzymes when a synthetic but not a natural substrate was used (Song et al., 2004; Pacholec et al., 2010). To avoid such artifacts, in this set of experiments the effect of His-Tyr and His-His on hydrolysis of three Nln substrates, neurotensin, angiotensin I, and bradykinin (Dauch et al., 1995; Rioli et al., 2003), was studied using mass spectrometry, and concentration-dependent effects were documented (Fig. 5). More specifically, formation of neurotensin-(1-10) from neurotensin in the presence of 40 and 100 μM His-Tyr was increased by 106% (95% CI, 70%–142%) and 180% (95% CI, 150%–209%) compared with Nln alone, and in the presence of 40 and 100 μM His-His it was increased by 83% (95% CI, 44%–122%) and 187% (95% CI, 160%–214%), respectively (Fig. 5). Formation of angiotensin-(1-7) from angiotensin I in the presence of 40 and 100 μM His-Tyr was increased by 93% (95% CI, 66%–119%) and 189% (95% CI, 144%–234%) compared with Nln alone, whereas in the presence of 40 and 100 μM His-His it was increased by 47% (95%

TABLE 2
The effect of top-ranking 40 compounds from NCI DTP on catalytic activity of recombinant rat Nln
Mean values from two independent experiments are shown. Structures and additional physicochemical information for these compounds can be found at https://dtp.cancer.gov/dtpstandard/dwindex/index.jsp based on their NSC number.

NSC #	**608820**	**615399**	**639022**	**640354**	**659264**	**296961**	**302851**	**332636**	**333568**	**339919**
Score ranking	13, 41, 44	34	54	32	49	48	10, 27, 56	46	23, 37	57
% activity at 10 μM[a]	102	108	91	79	104	106	104	103	106	100
% activity at 100 μM[a]	108	108	30	76	107	127	80	64	77	63
NSC #	**359097**	**374121**	**400844**	**523374**	**600947**	**353874**	**211002**	**266752**	**281707**	**282137**
Score ranking	5	35	30	7, 9, 22, 71	11, 45, 89	2	15	59, 83	14	36
% activity at 10 μM	87	121	104	122	107	122	104	107	109	106
% activity at 100 μM	92	226	84	206	105	80	100	97	113	94
NSC #	**343659**	**14541**	**15180**	**47096**	**134514**	**155877**	**163084**	**203396**	**210826**	**48778**
Score ranking	20	6	42	43, 99	21, 25, 40, 47	8	12	16	53	18, 73
% activity at 10 μM	105	97	102	101	92	82	103	102	101	89
% activity at 100 μM	106	103	95	111	9	4	102	106	105	84
NSC #	**82001**	**88659**	**89624**	**92597**	**121184**	**128977**	**131922**	**134119**	**340049**	**343028**
Score ranking	17	50	19, 38	51, 64	24	3	26, 39, 55, 82	31	33, 52	28, 29
% activity at 10 μM	105	100	102	105	77	80	96	83	94	98
% activity at 100 μM	100	100	38	98	18	68	28	41	52	73

[a]Compared with basal activity (i.e., vehicle control at 100%).

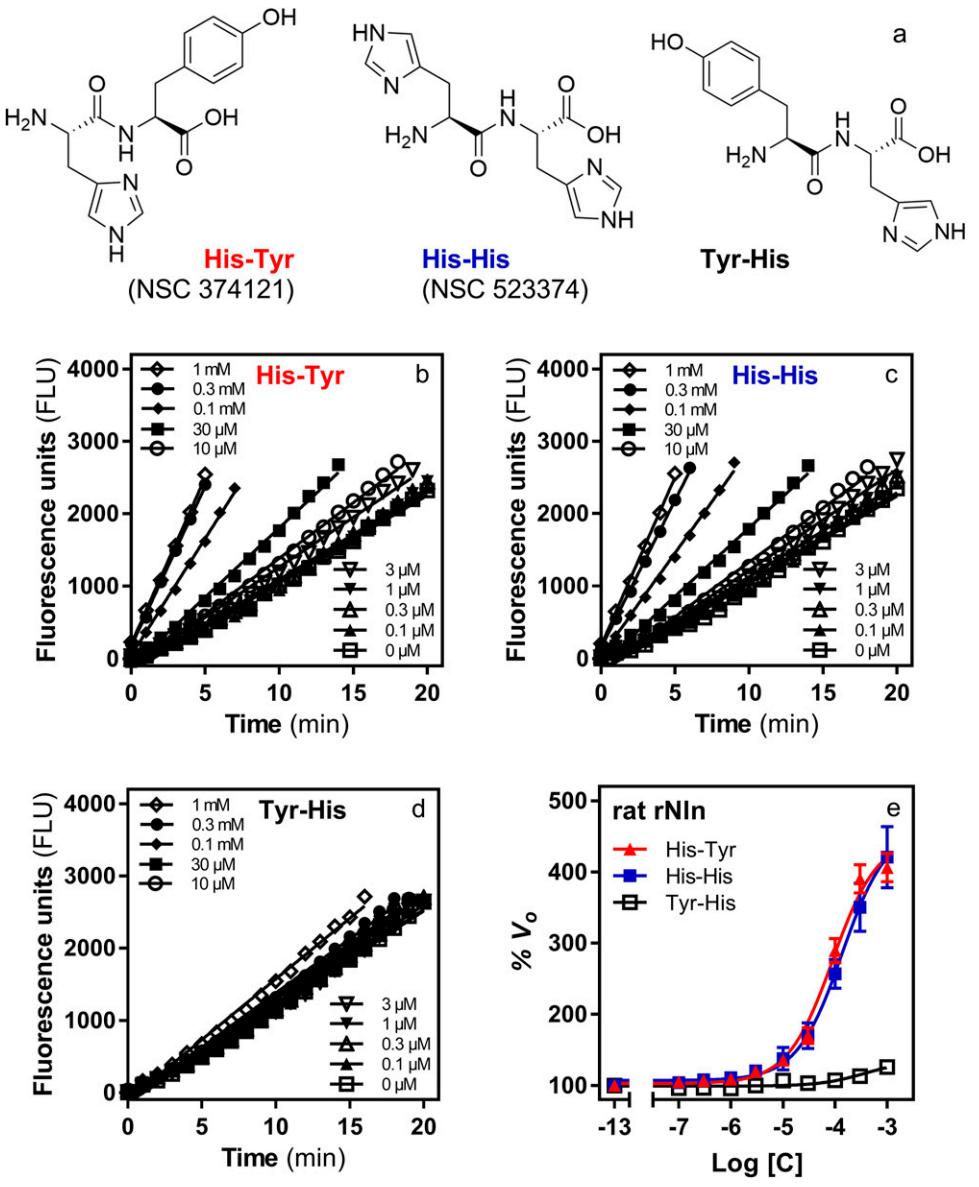

Fig. 2. The effect of dipeptides His-Tyr, His-His, and Tyr-His on catalytic activity of recombinant rat Nln. (A) Chemical structures of dipeptides His-Tyr (NSC 374121), His-His (NSC 523374), and Tyr-His. (B–D) Representative reaction progress curves of QFS hydrolysis (15 μM) by recombinant rat Nln (0.3 nM) in the presence of different concentrations of His-Tyr, His-His, and Tyr-His. (E) Concentration-dependent effect of all three dipeptides on hydrolysis of QFS under the same experimental conditions (mean ± S.D., n = 4 independent experiments with duplicate samples for each condition). Note that the initial velocity of hydrolysis in the absence of dipeptides corresponds to 100% on the vertical axis (basal activity) and −13 on the horizontal axis. For His-Tyr, A_{50} = 89.7 μM (95% CI, 74.2–108.6 μM) and A_{max} = 449% (95% CI, 432%–468%). For His-His, A_{50} = 136 μM (95% CI, 104–179 μM) and A_{max} = 463% (95% CI, 436%–492%). For Tyr-His, A_{50} = 355 μM (95% CI, 179–780 μM) and A_{max} = 135% (95% CI, 127%–149%).

CI, 30%–63.5%) and 153% (95% CI, 113%–193%), respectively. Lastly, in the presence of 40 and 100 μM His-Tyr, formation of bradykinin-(1-5) from bradykinin was increased by 65% (95% CI, 15%–115%) and 153% (95% CI, 97%–208%) compared with Nln alone, whereas in the presence of 40 and 100 μM His-His, formation of bradykinin-(1-5) was increased by 99% (95% CI, 80%–119%) and 227% (95% CI, 217%–317%), respectively.

Based on these data we further expanded our studies to gain more mechanistic understanding about activation of Nln by His-Tyr and His-His.

Effect of His-Tyr and His-His on Catalytic Efficiency of Nln. To determine whether the increased initial velocity of substrate hydrolysis by Nln in the presence of His-Tyr or His-His is attributable to increased catalytic efficiency of the peptidase, in this set of experiments the effect of both modulators on hydrolysis of synthetic substrate at different concentrations (spanning from ∼6-fold less to ∼5-fold more of its K_m value) was studied. In the presence of 40 μM His-Tyr maximal velocity (V_{max}) of the hydrolysis was increased by ∼29%, whereas K_m value was decreased by ∼43%, resulting in more than doubling of V_{max}/K_m ratio (Fig. 6; Table 3). Likewise, in the presence of His-His (40 μM) V_{max} value increased by ∼16.5%, whereas K_m value decreased by ∼42.4%, resulting in doubling of V_{max}/K_m ratio (Fig. 6; Table 3). The same trend was observed in the presence of 100 μM concentration of either dipeptide, resulting in more than tripling of V_{max}/K_m ratio (Fig. 6; Table 3).

The Modulatory Site on Nln Is Different from the Substrate Binding Site. To determine whether His-Tyr and His-His are interacting with a binding site on Nln that is different from the substrate binding site, a set of experiments was carried out using a competitive inhibitor of Nln, dynorphin A (1-13) (Rioli et al., 2003). In the first experiment, the effect of a fixed concentration of His-Tyr or His-His on the affinity of dynorphin A (1-13) (i.e., K_i value) in inhibiting Nln was determined (Fig. 7). As expected, both His-Tyr and His-His enhanced activity of Nln, and this effect was also observed

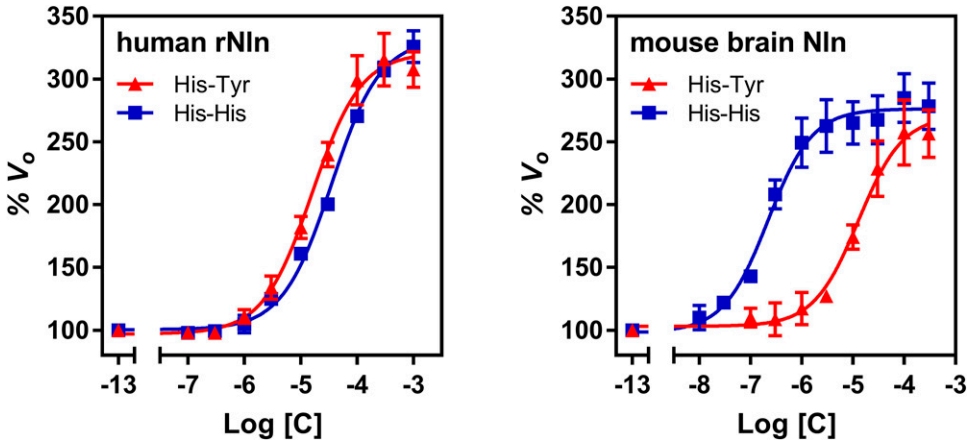

Fig. 3. The effect of His-Tyr and His-His on catalytic activity of recombinant human (left) and mouse brain–isolated (right) Nln. The panels document concentration-dependent effect of both compounds on hydrolysis of synthetic substrate at 15 μM (mean ± S.D., n = 4 independent experiments with duplicate samples for each condition). Note that the initial velocity of the hydrolysis in the absence of either compound corresponds to 100% on the vertical axis and −13 on the horizontal axis. With recombinant human Nln, A_{50} = 15.9 μM (95% CI, 13.0–19.3 μM) and A_{max} = 321% (95% CI, 313–330) for His-Tyr. For His-His, A_{50} = 35.1 μM (95% CI, 30.1–39.9 μM) and A_{max} = 332% (95% CI, 326%–338%). With mouse brain–isolated Nln, A_{50} = 12.7 μM (95% CI, 8.9–17.9 μM) and A_{max} = 271% (95% CI, 258%–285%) for His-Tyr. For His-His, A_{50} = 0.22 μM (95% CI, 0.16–0.29 μM) and A_{max} = 276% (95% CI, 269%–283%).

in the presence of dynorphin A (1-13) at concentrations close to its IC_{50} value and below. However, K_i values for dynorphin A (1-13) did not differ statistically significantly in the absence and presence of the activators: K_i value was 1.19 μM (95% CI, 1.03–1.38 μM) in the absence of the activators, it was 0.92 μM (95% CI, 0.76–1.12 μM) in the presence of 100 μM His-Tyr, and it was 0.93 μM (95% CI, 0.78–1.11 μM) in the presence of 100 μM His-His. In a reverse experiment, the concentration-response effect of His-Tyr and His-His on activity of Nln was studied in the absence and presence of a fixed concentration of dynorphin A (1-13) (Fig. 7). In these experiments, dynorphin A (1-13) inhibited activity of Nln and decreased A_{max} values of His-Tyr and His-His. However, it did not significantly affect the A_{50} values of the modulators (Fig. 7): A_{50} value for His-Tyr was 109.9 μM (95% CI, 86.3–141 μM) and 116 μM (95% CI, 91.5–151 μM) in the absence and presence of dynorphin A

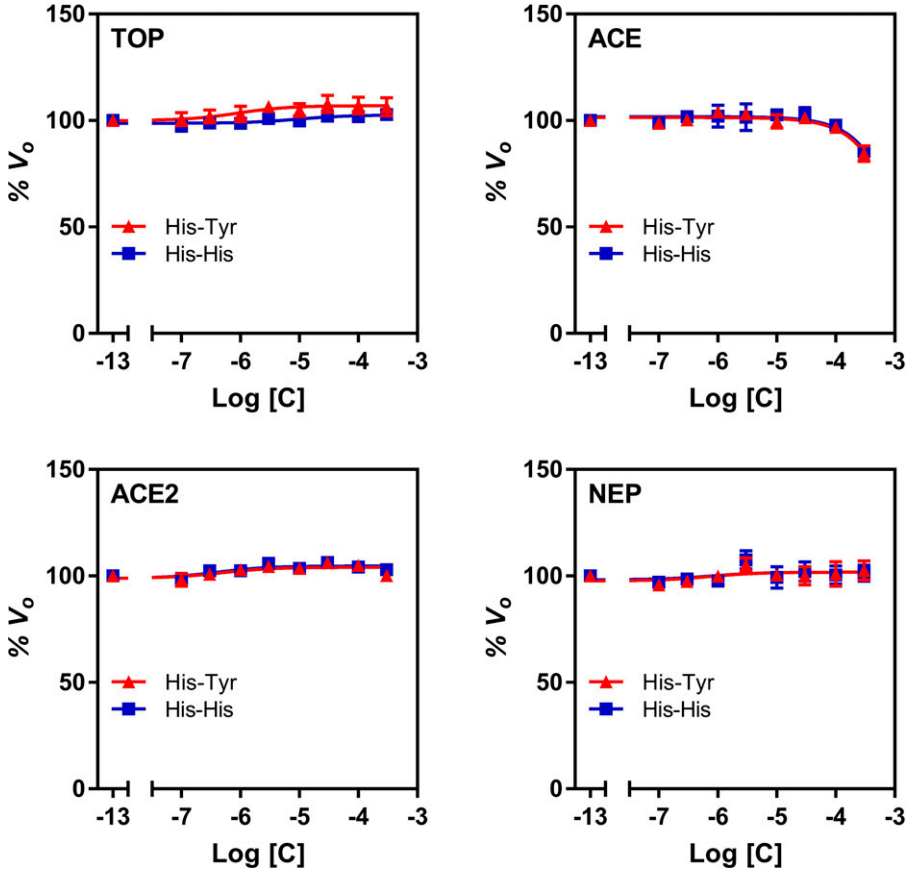

Fig. 4. The effect of His-Tyr and His-His on catalytic activity of recombinant human peptidases. All panels document concentration-dependent effect of His-Tyr and His-His on hydrolysis of a respective quenched fluorescence substrate (mean ± S.D., n = 4 independent experiments with duplicate samples for each condition): Mca-Pro-Leu-Gly-Pro-D-Lys(DNP)-OH at 15 μM for thimet oligopeptidase (TOP), Mca-Arg-Pro-Pro-Gly-Phe-Ser-Ala-Phe-Lys(Dnp)-OH at 10 μM for angiotensin converting enzyme (ACE) and neprilysin (NEP), and Mca-Ala-Pro-Lys-(Dnp)-OH at 10 μM for angiotensin converting enzyme 2 (ACE2). In all panels, the initial velocity of the hydrolysis in the absence of either compound corresponds to 100% on the vertical axis and −13 on the horizontal axis.

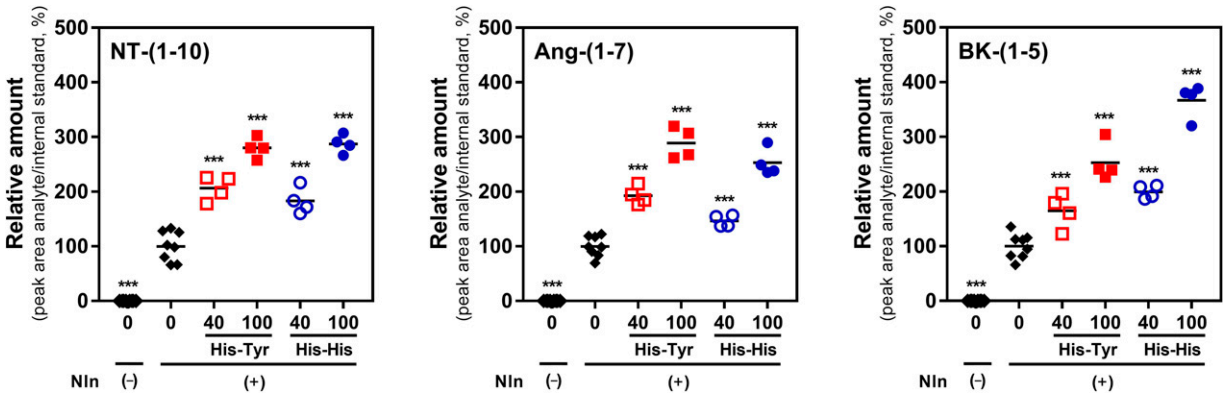

Fig. 5. The effect of His-Tyr and His-His on hydrolysis of bradykinin, angiotensin I, and neurotensin by Nln. Recombinant rat Nln (0.5 nM) was incubated with one of the endogenous peptides (20 μM) in the absence or presence of His-Tyr or His-His (40 or 100 μM). Formation of neurotensin-(1-10) [NT-(1-10)], angiotensin-(1-7) [Ang-(1-7)], and bradykinin-(1-5) [BK-(1-5)] was documented by mass-spectrometry analysis (n = 4 independent experiments with duplicate samples for controls and individual samples for each concentration of either dipeptide; ***, $P < 0.001$ in comparison with Nln alone). In all panels, "0 and Nln (–)" corresponds to a condition wherein the respective peptide substrate was incubated in assay buffer alone (i.e., no Nln, hence no product formation). Likewise, "0 with Nln (+)" corresponds to a condition wherein the respective peptide substrate was incubated in assay buffer with Nln alone (i.e., no activator molecule was present, corresponds to basal level of product formation). The black line within the scattered dots for each experimental group indicates the mean.

(1-13), respectively. A_{50} value for His-His was 132 μM (95% CI, 96.8–186 μM) and 158 μM (95% CI, 119–216 μM) in the absence and presence of dynorphin A (1-13), respectively.

Binding of His-Tyr to Nln Confirmed by DARTS Assay. To determine whether His-Tyr directly interacts with Nln, we used a well established technique—DARTS assay—that is widely used for identification of protein targets for new pharmacological agents (Lomenick et al., 2009). In the presence of His-Tyr (at 30, 100, and 300 μM) we observed a concentration-dependent protection of Nln degradation by subtilisin (Fig. 8). Compared with the density of undigested recombinant rat Nln exposed to vehicle but not subtilisin, the detectible amount of Nln incubated with vehicle and subtilisin was 12.7% (95% CI, 9.7%–15.7%). However, in samples in which Nln was incubated with His-Tyr and subtilisin, a gradual increase in density of Nln was documented: 11.6% (95% CI, 4.06%–19.1%), 21.1% (95% CI, 12.1%–30.2%), and 31.0% (95% CI, 24.3%–37.6%) for 30, 100, and 300 μM His-Tyr, respectively. To validate these observations, the same experiment was carried out using recombinant NEP—a closely related peptidase to Nln, activity of which is not affected by His-Tyr (Fig. 4). The results of these experiments revealed that degradation of NEP by subtilisin is not affected in the presence of the dipeptide (Fig. 8B); NEP density compared with undigested control was 26.6% (95% CI, 21.3%–31.9%), 25.8% (95% CI, 13.8%–37.8%), 25.3% (95% CI, 14.6% – 36.0%), and 30.8% (95% CI, 24.5%–37.0%) for vehicle and 30, 100, and 300 μM His-Tyr, respectively. As an additional control, we tested a competitive inhibitor of Nln dynorphin A (1-13) (DynA) using the same experimental design. As expected, in this experiment also, a concentration-dependent protection of Nln degradation was documented in the presence of DynA (Fig. 8); Nln density compared with undigested control was 11.9% (95% CI, 9.6%–14.0%), 19.7% (95% CI, 11.3%–28.1%), 27.4% (95% CI, 14.0%–40.8%), and 31.9% (95% CI, 29.1% – 34.7%) for vehicle and 30, 100, and 300 μM DynA, respectively.

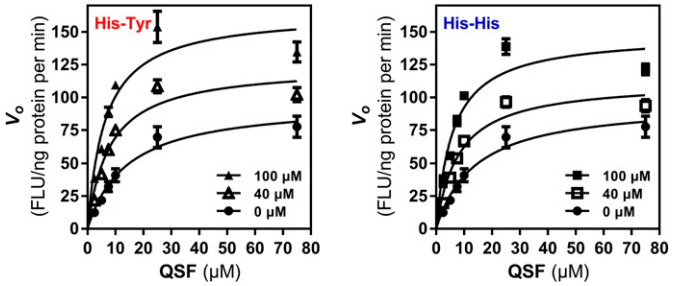

Fig. 6. The effect of His-Tyr and His-His on catalytic efficiency of Nln. Hydrolysis of different concentrations of synthetic substrate (QFS) by recombinant rat Nln (0.3 nM) in the absence or presence of His-Tyr and His-His (40 and 100 μM) is presented (mean ± S.D., n = 4 independent experiments with duplicate samples for each condition; FLU, fluorescence unit).

Interaction of His-Tyr with Nln Confirmed by DSF. To further validate binding of His-Tyr to Nln, we used another independent technique—DSF (also known as thermal shift assay)—that is widely used in screening of ligands and characterization of ligand and protein target interactions (Bai et al., 2019). In these experiments we observed a concentration-dependent shift in thermal unfolding transition of Nln toward lower temperature in the presence of His-Tyr (Fig. 9); the midpoint of the unfolding transition (i.e., melting temperature, T_m) was 60°C (95% CI, 60–60°C), 59.3°C (95% CI, 59.1–59.5°C), 57.5°C (95% CI, 57.2–57.9°C), and 54.1°C (95% CI, 53.9–54.3°C) for vehicle and 30, 100, and 300 μM His-Tyr, respectively. The same experiment carried out with NEP revealed no effect on thermal unfolding transition of this peptidase in the presence of His-Tyr (Fig. 9); T_m was 54.6°C (95% CI, 54.3–54.9°C), 54.5°C (95% CI, 54.2–54.8°C), 54.5°C (95% CI, 54.2–54.8°C), and 54.5°C (95% CI, 54.2–54.8°C) for vehicle and 30, 100, and 300 μM His-Tyr, respectively. Similar to DARTS assays, here too, we carried out additional experiments with Nln and competitive inhibitor DynA and observed a concentration-dependent shift in thermal unfolding transition of Nln toward higher temperature (Fig. 9); T_m was 60.5 (95% CI, 60.5–60.5°C), 60.8°C (95% CI, 60.6–61.0°C), 61.5°C (95% CI, 61.5–61.5°C), and 62.5°C (95% CI, 62.5–62.5°C) for vehicle and 30, 100, and 300 μM DynA, respectively.

TABLE 3
Calculated V_{max} and K_m values for experiments presented in Figure 6
V_{max} units are in FLU/ng protein per min, K_m units are in μM (FLU, fluorescence unit). Data are presented as means together with 95% confidence intervals in parentheses (n = 4 independent experiments with duplicate samples for each condition; *$P < 0.05$; ***$P < 0.001$ in comparison with Nln values).

	V_{max}	K_m	V_{max}/K_m	Fold Change
Nln	96.6 (91.3–101.8)	13.9 (12.0 –15.8)	6.9	—
Nln + 40μM His-Tyr	124.2*** (112.2–136.2)	7.9*** (5.7–10.1)	15.7	2.3
Nln + 100μM His-Tyr	164.8*** (147.2–182.4)	6.4*** (4.3–8.5)	25.8	3.7
Nln + 40μM His-His	112.5* (102.7–122.3)	8.0*** (6.0–10.0)	14.0	2.0
Nln + 100μM His-His	148.2*** (133.0–163.3)	6.1*** (4.1–8.0)	24.4	3.5

Discussion

In this study we have identified and characterized two structurally related dipeptides that enhance catalytic efficiency of peptidase Nln. For this we explored the hinge region of Nln to identify a potentially druggable site, and this was followed by docking and in silico screening of ~140,000 small molecules from NCI DTP (Fig. 1; Table 1). The compounds were ranked based on their combined energy scores for hydrogen bonding and van der Waals contact interactions with the Nln hinge region surface pocket. The highest-ranking 40 compounds were screened to evaluate their effect on the rate of synthetic substrate hydrolysis by recombinant Nln, and dipeptides His-Tyr and His-His were identified as potential activators (Table 2). Potencies (A_{50} values) of the identified dipeptides were ~100 μM with A_{max} values ≥400% for hydrolysis of the synthetic substrate by recombinant rat Nln (Fig. 2). The observed effects were reproducible in an assay buffer supplemented with Triton X-100 or CHAPS or BSA, all of which are methodological tactics recommended for preventing identification of promiscuous enzyme modulators (Supplemental Fig. 1). The inherent fluorescence-enhancing or -quenching characteristics of His-Tyr and His-His were evaluated, revealing lack of such properties (Supplemental Fig. 1). Additionally, we tested the effect of Tyr-His, a reverse sequence analog of His-Tyr, but only documented negligible effect on activity of Nln (Fig. 2). His-Tyr and His-His also enhanced, albeit with different potencies, activity of recombinant human and mouse brain–purified Nln (Fig. 3), indicating that activation of Nln is not limited to the recombinant peptidase and that the Nln binding site of activators is conserved/similar among these species. On the contrary, His-Tyr and His-His had negligible effect on activity of peptidases closely related to Nln, including TOP, NEP, ACE, and ACE2 (Fig. 4). Although we did not test all known pharmacological targets, the negligible effect of His-Tyr and His-His on activity of four closely related peptidases suggests that these molecules possess excellent selectivity for Nln and do not promiscuously enhance activity of peptidases. To determine whether the effect of His-Tyr and His-His on activity of Nln was observed only with the synthetic substrate, hydrolysis of endogenous substrates was evaluated (Fig. 5). These experiments revealed that both dipeptides enhanced hydrolysis of neurotensin, angiotensin I, and bradykinin by Nln, suggesting that the effect of activators was specific to the peptidase and not limited to the synthetic substrate. In separate experiments, we also determined that the dipeptides increase catalytic efficiency (V_{max}/K_m ratio) of Nln in a concentration-dependent manner by reducing K_m and increasing V_{max} values (Fig. 6; Table 3).

To check whether His-Tyr and His-His interact with a binding pocket that is different from the substrate binding site in Nln, we conducted experiments with dynorphin A (1-13), a competitive inhibitor of the peptidase (Rioli et al., 2003). These observations revealed that dynorphin A (1-13) and His-Tyr or His-His interact with different binding sites on Nln because they did not

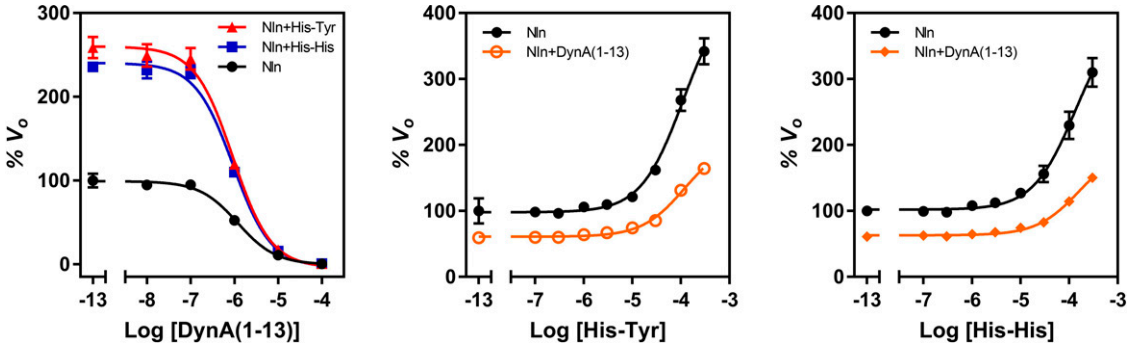

Fig. 7. Reciprocal effects of His-Tyr or His-His and competitive inhibitor dynorphin A (1-13) on activity of Nln. Left panel presents concentration-dependent inhibitory effect of dynorphin A (1-13) on hydrolysis of synthetic substrate (15 μM) by recombinant rat Nln (0.3 nM) in the absence or presence of His-Tyr or His-His (100 μM) (mean ± S.D., n = 4 independent experiments with duplicate samples for each condition). Calculated IC_{50} values for dynorphin A (1-13) are 1.2 μM (95% CI, 1.03–1.38 μM) in Nln, 0.92 μM (95% CI, 0.76–1.12 μM) in Nln + His-Tyr, and 0.93 μM (95% CI, 0.78–1.11 μM) in Nln + His-His. Center and right panels present concentration-dependent effect of His-Tyr and His-His on hydrolysis of synthetic substrate (15 μM) by recombinant rat Nln (0.3 nM) in the absence or presence of dynorphin A (1-13) (1 μM) (mean ± S.D., n = 4 independent experiments with duplicate samples for each condition). Calculated A_{50} values for His-Tyr are 109.9 μM (95% CI, 86.3 – 141 μM) and 116 μM (95% CI, 91.5 –151 μM) in the absence and presence of dynorphin A (1-13), respectively. Corresponding A_{max} values for His-Tyr are 435% (95% CI, 406%–472%) and 206% (95% CI, 193%–223%). Calculated A_{50} values for His-His are 132 μM (95% CI, 96.8–186 μM) and 158 μM (95% CI, 119–216 μM) in the absence and presence of dynorphin A (1-13), respectively. Corresponding A_{max} values for His-His are 401% (95% CI, 366%–448%) and 196% (95% CI, 181%–217%). Note that the initial velocity of hydrolysis in the absence of any ligand corresponds to 100% on the vertical axis and −13 on the horizontal axis in these panels.

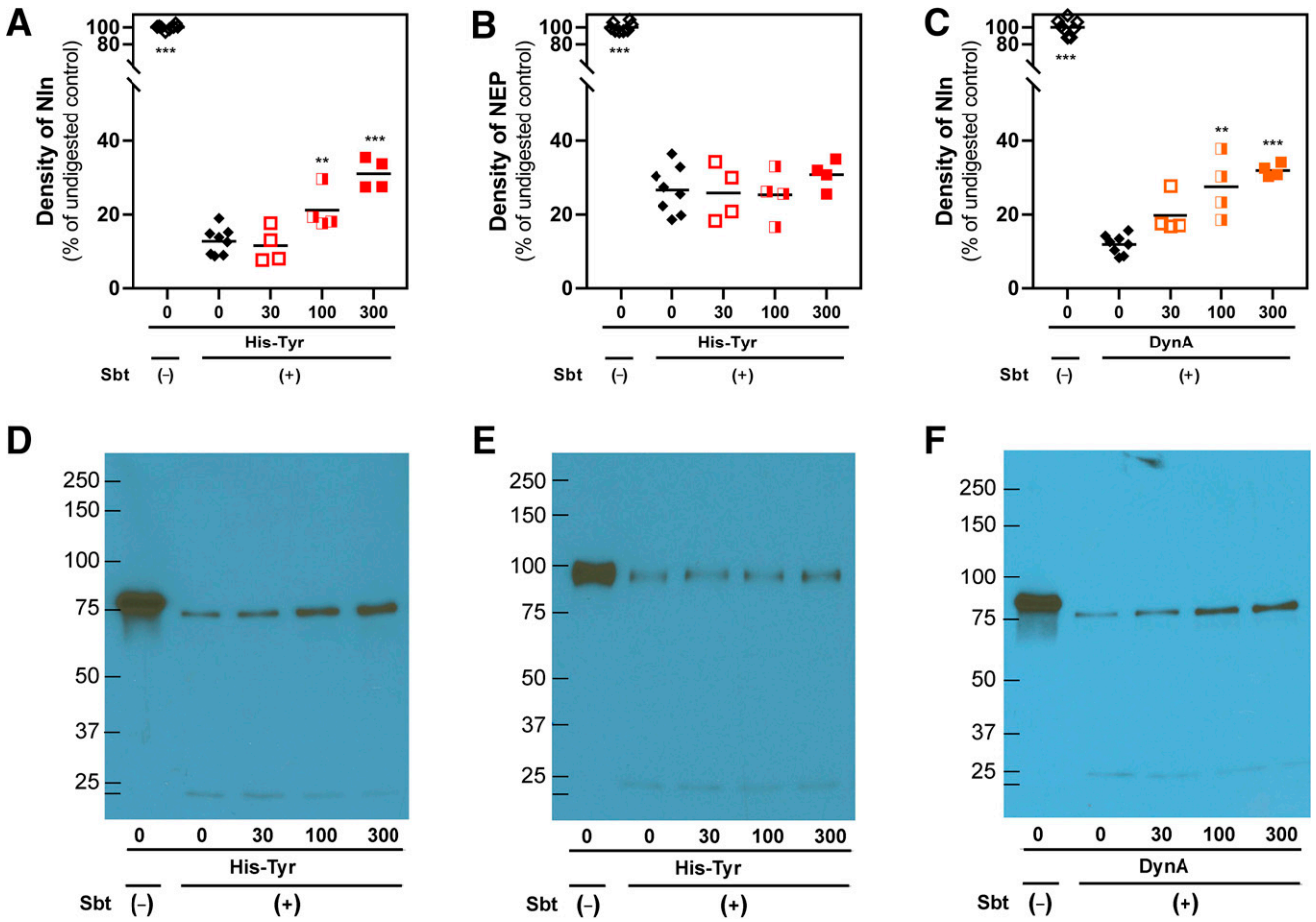

Fig. 8. DARTS analysis of His-Tyr and Nln interaction. (A and B) present concentration-dependent effect of His-Tyr (at 30, 100, and 300 μM) on degradation of recombinant Nln (A; 2.6 μM) and NEP (B; 2.6 μM) by subtilisin A (Sbt). In the presence of His-Tyr statistically significant protection of Nln digestion is observed (A), which, however, is lacking in NEP under the same experimental conditions (B). (C) presents concentration-dependent effect of Nln inhibitor dynorphin A (1-13) (DynA, at 30, 100, and 300 μM) on degradation of recombinant Nln by subtilisin A. Here too, digestion of Nln is diminished in the presence of DynA, which is a known competitive inhibitor of the peptidase (n = 4 independent experiments with duplicate samples for controls and individual samples for each concentration of a ligand; **, $P < 0.01$, ***, $P < 0.001$ compared with digested peptidase incubated with vehicle and subtilisin A). The black line within the scattered dots for each experimental group indicates the mean. (D-F) representative results of immunoblotting experiments based on which the degree of degradation (i.e., density) for Nln and NEP were measured in the experimental groups.

affect each other's affinity for the peptidase (Fig. 7). Although A_{50} value does not directly indicate ligand affinity, in these experiments wherein all variables were maintained unchanged (concentrations of substrate, activators, Nln, etc.), the documented A_{50} values for the dipeptides in the absence and presence of dynorphin A (1-13) suggest that their affinity for Nln remained unaffected. Because dynorphin A (1-13) is a competitive inhibitor of Nln, these data also suggest that the activator binding site is different from the substrate binding site.

Since the observed effects of both dipeptides were comparable throughout the above-described studies, next we focused on His-Tyr alone and used two additional techniques, DARTS and DSF, to document interaction of His-Tyr with Nln. DARTS results confirmed the expected concentration-dependent protection of Nln from proteolytic degradation by a known [dynorphin A (1-13)] and new (His-Tyr) ligand (Fig. 8). Consistent with this, the protective effect of His-Tyr was absent in NEP (because this dipeptide is not a NEP ligand), and indicated that His-Tyr does not affect activity of subtilisin. Similarly, DSF experiments revealed that both dynorphin A (1-13) and His-Tyr interact with Nln and affect its midpoint of unfolding transition (T_m; Fig. 9). On the contrary, this effect of His-Tyr was absent in NEP, indicating lack of substantial interaction between these two molecules. The shift in T_m of Nln toward lower temperature in the presence of His-Tyr is notable, because in most cases ligand-protein interaction leads to transition of T_m to higher temperature (Bai et al., 2019), as observed with dynorphin A (1-13). However, downward shift of T_m upon ligand binding has been documented for various targets, including enzymes (e.g., isocitrate lyase) (Sharma et al., 2000). These observations led to suggestions that positive thermal shift may indicate adaptation of a more stable "closed" conformation upon ligand binding, whereas a negative thermal shift may be observed when the ligand leads or maintains the target protein in a less stable "open" conformation (Sharma et al., 2000; Cimmperman et al., 2008). This question warrants future studies, likely X-ray crystallography with high-affinity Nln activators, to obtain insight about activator binding and activation mechanism(s). Unfortunately, our efforts to co-crystallize Nln with His-Tyr have not been successful so far. One likely reason is the modest affinity of His-Tyr for Nln, which is suboptimal for X-ray crystallography. In addition, the

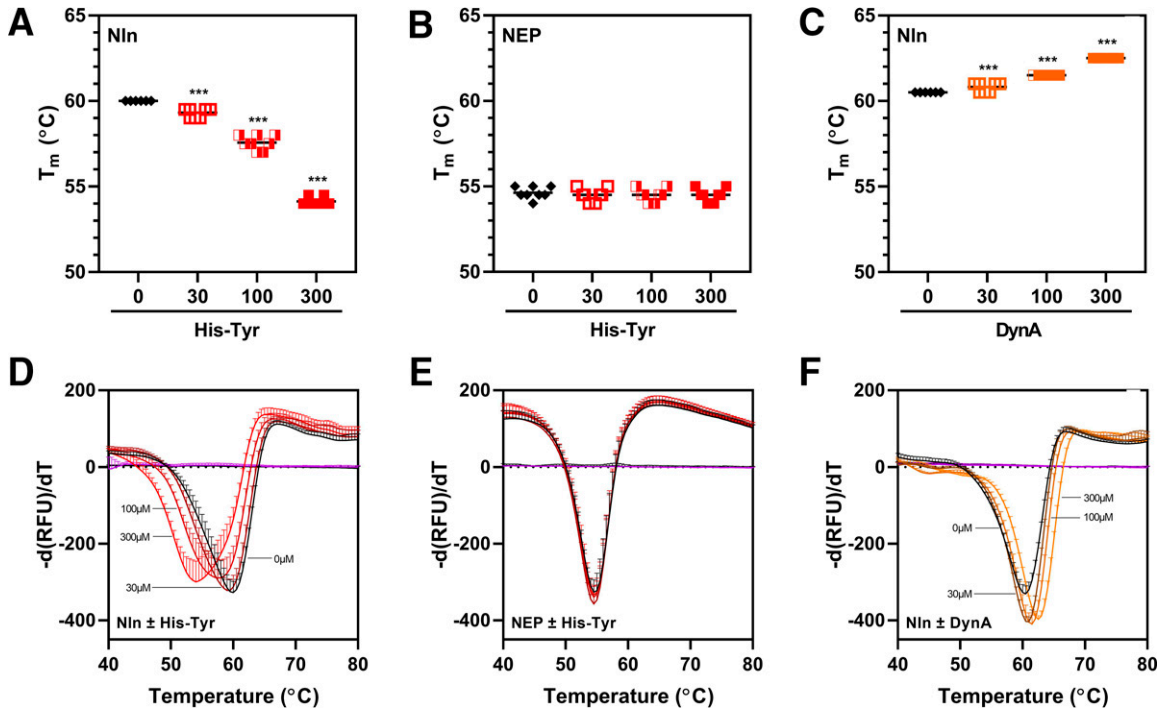

Fig. 9. DSF analysis of His-Tyr and Nln interaction. (A and B) present concentration-dependent effect of His-Tyr (at 30, 100, and 300 μM) on midpoint of the unfolding transition (i.e., melting temperature, T_m) of recombinant Nln (A; 3 μM) and NEP (B; 3 μM). In the presence of His-Tyr, a statistically significant shift of Nln T_m toward lower temperature is observed (A), whereas NEP T_m is not affected under the same experimental conditions (B). (C) presents concentration-dependent effect of Nln inhibitor dynorphin A (1-13) (DynA, at 30, 100, and 300 μM) on Nln T_m. In this case, a statistically significant shift of Nln T_m toward higher temperature is observed in the presence of DynA [n = 4 independent experiments with duplicate samples for each condition; ***, $P < 0.001$ compared with a control condition wherein the respective peptidase was incubated with vehicle (0)]. The black line within the scattered dots for each experimental group indicates the mean. (D–F) Summary of negative derivative [d(RFU)/dT] curves for (A–C) are shown (RFU, relative fluorescence unit).

enhanced dynamics of Nln in the presence of His-Tyr might have also contributed to the challenges of crystallographic experiments. The latter issue has been well recognized in the field of enzyme activators since very few structures of activator-bound enzymes have been characterized (Zorn and Wells, 2010). Our ongoing efforts focus on development of high-affinity Nln activators based on structures of His-Tyr and His-His with a goal to cocrystallize these ligands with Nln to confirm the predicted activator binding site and elucidate the potential activation mechanism.

The dipeptidic nature of the identified Nln activators is notable. The first selective Nln inhibitors described in literature were proline-containing dipeptides (Dauch et al., 1991b), of which *L*-prolyl-*L*-isoleucine was the most potent and is still used as a research tool. Based on our data, it is reasonable to predict that N-terminal histidine or part of its molecule is the main pharmacophore in both dipeptides. However, the role of the C-terminal amino acid in binding of the molecule to Nln and modulation of its activity cannot be excluded. Indeed, our detailed structure-activity studies to understand this relationship answer these questions and further validate the identified hit dipeptide scaffolds (Rahman et al., 2021). Our ongoing studies focus on design of peptidomimetic and bioisosteric lead structures and give us confidence that rational medicinal-chemical approaches will allow development of high-potency Nln activators with optimal drug-like properties for proof-of-concept in vivo studies and likely drug development.

In summary, this is the first study to demonstrate that activity of Nln can be enhanced by small molecules and describe two dipeptides that possess such properties. Our inability to confirm the predicted binding site of these dipeptides is the main limitation of this study but remains the focus of our ongoing efforts. Regrettably, the low potency and unfavorable drug-like properties of the identified dipeptides prevented us from conducting proof-of-concept in vivo studies and evaluating the cerebroprotective potential of these molecules. Despite this, we firmly believe that high-potency, drug-like Nln activators, which are being actively developed by our research team (Rahman et al., 2021), could become important research tools to study functional significance of Nln in various (patho)physiologic conditions. As deliberated in more detail in the introduction section of this manuscript, recent experimental studies have suggested that Nln is a compensatory, cerebroprotective mechanism in the poststroke brain functioning to inactivate cerebrotoxic and generate neuroprotective peptides (Jayaraman et al., 2020; Karamyan, 2021b). The ability of Nln to process multiple neuropeptides suggests that pharmacological modulation of its activity could potentially translate to changes in the function of the same peptidergic systems (Al-Ahmad et al., 2021). Nln could serve as a single therapeutic target to modulate the function of multiple targets. Such multipathway targets would be highly desired for stroke pharmacotherapy since it is well-recognized that targeting one pathophysiological pathway is unlikely to be therapeutically effective in this complex disorder. If the therapeutic potential of Nln activators is confirmed in future studies, such molecules could become a new drug class for stroke therapy and perhaps other neurologic disorders (Karamyan, 2019, 2021a). Hence,

the identified dipeptides provide a chemical scaffold for the development of high-potency, drug-like molecules as research tools and potential drug leads.

Acknowledgments

The authors thank Dr. David W. Rodgers, University of Kentucky, for the gift of the plasmid vector construct for rat Nln. The tested compounds in this study were obtained from the National Cancer Institute (NCI) Division of Cancer Treatment and Diagnosis, Developmental Therapeutics Program (http://dtp.cancer.gov).

Authorship Contributions

Participated in research design: Jayaraman, Kocot, Hadi Esfahani, Aihara, Ostrov, Karamyan.

Conducted experiments: Jayaraman, Kocot, Hadi Esfahani, Ostrov, Karamyan.

Contributed new reagents or analytic tools: Wangler, Uyar, Mechref, Dickson, Aihara.

Performed data analysis: Jayaraman, Kocot, Hadi Esfahani, Ostrov, Karamyan.

Wrote or contributed to the writing of the manuscript: Jayaraman, Kocot, Hadi Esfahani, Trippier, Abbruscato, Ostrov, Karamyan.

References

Al-Ahmad AJ, Pervaiz I, and Karamyan VT (2021) Neurolysin substrates bradykinin, neurotensin and substance P enhance brain microvascular permeability in a human in vitro model. *J Neuroendocrinol* **33**:e12931.

Bai N, Roder H, Dickson A, and Karanicolas J (2019) Isothermal analysis of ThermoFluor data can readily provide quantitative binding affinities. *Sci Rep* **9**:2650.

Brown CK, Madauss K, Lian W, Beck MR, Tolbert WD, and Rodgers DW (2001) Structure of neurolysin reveals a deep channel that limits substrate access. *Proc Natl Acad Sci USA* **98**:3127–3132.

Checler F and Ferro ES (2018) Neurolysin: from initial detection to latest advances. *Neurochem Res* **43**:2017–2024.

Cimmperman P, Baranauskiene L, Jachimoviciūte S, Jachno J, Torresan J, Michailoviene V, Matuliene J, Sereikaite J, Bumelis V, and Matulis D (2008) A quantitative model of thermal stabilization and destabilization of proteins by ligands. *Biophys J* **95**:3222–3231.

Dauch P, Barelli H, Vincent JP, and Checler F (1991a) Fluorimetric assay of the neurotensin-degrading metalloendopeptidase, endopeptidase 24.16. *Biochem J* **280**:421–426.

Dauch P, Vincent JP, and Checler F (1991b) Specific inhibition of endopeptidase 24.16 by dipeptides. *Eur J Biochem* **202**:269–276.

Dauch P, Vincent JP, and Checler F (1995) Molecular cloning and expression of rat brain endopeptidase 3.4.24.16. *J Biol Chem* **270**:27266–27271.

Dundas J, Ouyang Z, Tseng J, Binkowski A, Turpaz Y, and Liang J (2006) CASTp: computed atlas of surface topography of proteins with structural and topographical mapping of functionally annotated residues. *Nucleic Acids Res* **34**:W116–W118.

Feng BY, Shelat A, Doman TN, Guy RK, and Shoichet BK (2005) High-throughput assays for promiscuous inhibitors. *Nat Chem Biol* **1**:146–148.

Feng BY, Simeonov A, Jadhav A, Babaoglu K, Inglese J, Shoichet BK, and Austin CP (2007) A high-throughput screen for aggregation-based inhibition in a large compound library. *J Med Chem* **50**:2385–2390.

Goode DR, Totten RK, Heeres JT, and Hergenrother PJ (2008) Identification of promiscuous small molecule activators in high-throughput enzyme activation screens. *J Med Chem* **51**:2346–2349.

Hernández Prada JA, Ferreira AJ, Katovich MJ, Shenoy V, Qi Y, Santos RA, Castellano RK, Lampkins AJ, Gubala V, Ostrov DA, et al. (2008) Structure-based identification of small-molecule angiotensin-converting enzyme 2 activators as novel antihypertensive agents. *Hypertension* **51**:1312–1317.

Jayaraman S, Al Shoyaib A, Kocot J, Villalba H, Alamri FF, Rashid M, Wangler NJ, Chowdhury EA, German N, Arumugam TV, et al. (2020) Peptidase neurolysin functions to preserve the brain after ischemic stroke in male mice. *J Neurochem* **153**:120–137.

Joyner JC, Hocharoen L, and Cowan JA (2012) Targeted catalytic inactivation of angiotensin converting enzyme by lisinopril-coupled transition-metal chelates. *J Am Chem Soc* **134**:3396–3410.

Kabsch W and Sander C (1983) Dictionary of protein secondary structure: pattern recognition of hydrogen-bonded and geometrical features. *Biopolymers* **22**:2577–2637.

Karamyan VT (2019) Peptidase neurolysin is an endogenous cerebroprotective mechanism in acute neurodegenerative disorders. *Med Hypotheses* **131**:109309.

Karamyan VT (2021a) Between two storms, vasoactive peptides or bradykinin underlie severity of COVID-19? *Physiol Rep* **9**:e14796.

Karamyan VT (2021b) The role of peptidase neurolysin in neuroprotection and neural repair after stroke. *Neural Regen Res* **16**:21–25.

Kulemina LV and Ostrov DA (2011) Prediction of off-target effects on angiotensin-converting enzyme 2. *J Biomol Screen* **16**:878–885.

Lian W, Chen G, Wu D, Brown CK, Madauss K, Hersh LB, and Rodgers DW (2000) Crystallization and preliminary analysis of neurolysin. *Acta Crystallogr D Biol Crystallogr* **56**:1644–1646.

Lipinski CA, Lombardo F, Dominy BW, and Feeney PJ (2001) Experimental and computational approaches to estimate solubility and permeability in drug discovery and development settings. *Adv Drug Deliv Rev* **46**:3–26.

Lomenick B, Hao R, Jonai N, Chin RM, Aghajan M, Warburton S, Wang J, Wu RP, Gomez F, Loo JA, et al. (2009) Target identification using drug affinity responsive target stability (DARTS). *Proc Natl Acad Sci USA* **106**:21984–21989.

Miners JS, Verbeek MM, Rikkert MO, Kehoe PG, and Love S (2008) Immunocapture-based fluorometric assay for the measurement of neprilysin-specific enzyme activity in brain tissue homogenates and cerebrospinal fluid. *J Neurosci Methods* **167**:229–236.

Novinec M, Korenč M, Caflisch A, Ranganathan R, Lenarčič B, and Baici A (2014) A novel allosteric mechanism in the cysteine peptidase cathepsin K discovered by computational methods. *Nat Commun* **5**:3287.

Pacholec M, Bleasdale JE, Chrunyk B, Cunningham D, Flynn D, Garofalo RS, Griffith D, Griffor M, Loulakis P, Pabst B, et al. (2010) SRT1720, SRT2183, SRT1460, and resveratrol are not direct activators of SIRT1. *J Biol Chem* **285**:8340–8351.

Rahman MS, Kumari S, Esfahani SH, Nozohouri S, Jayaraman S, Kinarivala N, Kocot J, Baez A, Farris D, Abbruscato TJ, Karamyan VT and Trippier PC (2021) Discovery of first-in-class peptidomimetic neurolysin activators possessing enhanced brain penetration and stability. *J Med Chem* (re-submitted after minor revisions on August 5, 2021).

Rashid M, Arumugam TV, and Karamyan VT (2010) Association of the novel non-AT1, non-AT2 angiotensin binding site with neuronal cell death. *J Pharmacol Exp Ther* **335**:754–761.

Rashid M, Wangler NJ, Yang L, Shah K, Arumugam TV, Abbruscato TJ, and Karamyan VT (2014) Functional up-regulation of endopeptidase neurolysin during post-acute and early recovery phases of experimental stroke in mouse brain. *J Neurochem* **129**:179–189.

Ray K, Hines CS, Coll-Rodriguez J, and Rodgers DW (2004) Crystal structure of human thimet oligopeptidase provides insight into substrate recognition, regulation, and localization. *J Biol Chem* **279**:20480–20489.

Rioli V, Gozzo FC, Heimann AS, Linardi A, Krieger JE, Shida CS, Almeida PC, Hyslop S, Eberlin MN, and Ferro ES (2003) Novel natural peptide substrates for endopeptidase 24.15, neurolysin, and angiotensin-converting enzyme. *J Biol Chem* **278**:8547–8555.

Sharma V, Sharma S, Hoener zu Bentrup K, McKinney JD, Russell DG, Jacobs Jr WR, and Sacchettini JC (2000) Structure of isocitrate lyase, a persistence factor of Mycobacterium tuberculosis. *Nat Struct Biol* **7**:663–668.

Shrimpton CN, Glucksman MJ, Lew RA, Tullai JW, Margulies EH, Roberts JL, and Smith AI (1997) Thiol activation of endopeptidase EC 3.4.24.15. A novel mechanism for the regulation of catalytic activity. *J Biol Chem* **272**:17395–17399.

Shrimpton CN, Smith AI, and Lew RA (2002) Soluble metalloendopeptidases and neuroendocrine signaling. *Endocr Rev* **23**:647–664.

Song ES, Juliano MA, Juliano L, Fried MG, Wagner SL, and Hersh LB (2004) ATP effects on insulin-degrading enzyme are mediated primarily through its triphosphate moiety. *J Biol Chem* **279**:54216–54220.

Towler P, Staker B, Prasad SG, Menon S, Tang J, Parsons T, Ryan D, Fisher M, Williams D, Dales NA, et al. (2004) ACE2 X-ray structures reveal a large hinge-bending motion important for inhibitor binding and catalysis. *J Biol Chem* **279**:17996–18007.

Uyar A, Karamyan VT, and Dickson A (2018) Long-range changes in neurolysin dynamics upon inhibitor binding. *J Chem Theory Comput* **14**:444–452.

Vickers C, Hales P, Kaushik V, Dick L, Gavin J, Tang J, Godbout K, Parsons T, Baronas E, Hsieh F, et al. (2002) Hydrolysis of biological peptides by human angiotensin-converting enzyme-related carboxypeptidase. *J Biol Chem* **277**:14838–14843.

Wangler NJ, Jayaraman S, Zhu R, Mechref Y, Abbruscato TJ, Bickel U, and Karamyan VT (2016) Preparation and preliminary characterization of recombinant neurolysin for in vivo studies. *J Biotechnol* **234**:105–115.

Wangler NJ, Santos KL, Schadock I, Hagen FK, Escher E, Bader M, Speth RC, and Karamyan VT (2012) Identification of membrane-bound variant of metalloendopeptidase neurolysin (EC 3.4.24.16) as the non-angiotensin type 1 (non-AT1), non-AT2 angiotensin binding site. *J Biol Chem* **287**:114–122.

Zorn JA and Wells JA (2010) Turning enzymes ON with small molecules. *Nat Chem Biol* **6**:179–188.

Address correspondence to: Dr. Vardan T. Karamyan, 1300 Coulter St., Amarillo, TX 79106. E-mail: vardan.karamyan@ttuhsc.edu